Journal of Materials Chemistry B

Accepted Manuscript

ROYAL SOCIETY OF CHEMISTRY

www.rsc.org/materialsB

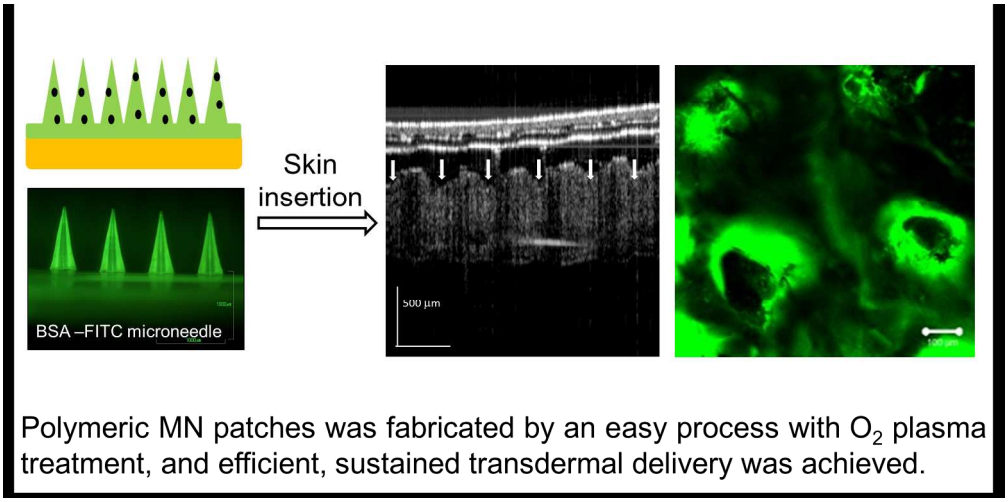

Polymeric MN patches was fabricated by an easy process with O_2 plasma treatment, and efficient, sustained transdermal delivery was achieved.

409x202mm (150 x 150 DPI)

Fabrication of a novel partial dissolving polymer microneedle patch for transdermal drug delivery

I-Chi Lee[1]*, Jheng-Siou He[1], Meng-Tsan Tsai[2#], Kai-Che Lin[1]

[1]Graduate Institute of Biochemical and Biomedical Engineering,

Chang-Gung University,

Tao-yuan 333, Taiwan, R.O.C.

[2]Department of Electrical Engineering,

Chang-Gung University,

Tao-yuan 333, Taiwan, R.O.C.

***Correspondence should be addressed to Dr. I-Chi Lee**

Phone: +886 3 2118800 ext 5985 Email: iclee@mail.cgu.edu.tw

[#]Co-corresponding author: Dr. Meng-Tsan Tsai

Phone: 886-3-2118800 ext 3732 Email: mttsai@mail.cgu.edu.tw

Abstract

Polymer microneedles (MNs) have gained increasing attention as a minimally invasive method for efficiently delivering drugs and vaccines in a patient-friendly manner. Herein, an easy and mild process with O_2 plasma treatment was used to fabricate polyvinylpyrrolidone (PVP)/polyvinyl alcohol (PVA) MN patches, and efficient, sustained transdermal delivery was achieved. The diffusion rate of the entrained molecules could be controlled by adjusting the ratio of PVP/PVA. Optical coherence tomography was used to monitor the in vitro penetration in real time and to measure the penetration depth.

Rhodamine 6G and fluorescein isothiocyanate-labeled bovine serum albumin (BSA-FITC) were used to explore the potential for using partial dissolving MNs as a transdermal delivery device. Confocal microscopy images revealed that the model drug can gradually diffuse from the puncture sites to a deeper depth. The drug-release profile also demonstrated that the PVP/PVA MNs can provide a successful and sustained release and that the transdermal delivery rate was regulated by the PVP/PVA ratio. Furthermore, the two-stage processing strategy developed in this study provides a simple and easy method for localizing the drug in the needle. The partial dissolving MNs developed in this study may serve a promising device for controlled drug release and for biological storage applications.

Keywords: partial dissolving polymer microneedle patch; plasma treatment; sustained release; optical coherence tomography; transdermal delivery rate

Introduction

Transdermal drug delivery is an attractive approach for the delivery of therapeutic agents due to its easy operation and to the avoidance of drug degradation in the gastrointestinal tract [1]. However, the substances that can be delivered via transdermal routes are limited to small (< 500 Da) and moderately hydrophobic compounds because the stratum cornea is the main barrier for drug penetration [2]. Microneedle (MN) arrays provide a pain-free alternative to increase skin permeability and enhance transdermal delivery [3]. This technology could be used to deliver a broad range of therapeutic macromolecules across the skin surface and epidermis in a minimally invasive manner by creating microscopic holes through which drugs diffuse to the dermal microcirculation [4, 5]. MNs should be designed such that they are long enough to penetrate to the dermis but sufficiently short and narrow to avoid stimulating dermal nerves [3].

The development of MN arrays currently faces challenges, including the selection of biomaterial, the harsh processing conditions that limit the types of drugs that can be used, and the inability to precisely control the kinetics and rate of drug release [6]. Polymer MNs are an attractive option for drug delivery because of their low cost and easy fabrication through micromolding processes, which allows for their mass production. Polymer MNs have recently been demonstrated to enhance the efficiency of transdermal delivery of a wide range of hydrophilic molecules, particularly macromolecules and high-molecular-weight proteins[7-10]. Among these MNs, water-soluble and biodegradable polymers eliminate the risk of MNs remaining in the skin and also ensure the safe disposal of MNs via degradation or dissolution in a solvent[11-14]. Specifically, dissolving polymer MNs fabricated from polyvinylpyrrolidone (PVP), polyvinyl alcohol (PVA), carboxymethyl cellulose, and poly(methyl vinyl ether co-maleic acid), which can avoid the use of harsh fabrication

methods such as high temperatures and organic solvents, have recently been highlighted [7, 8, 15, 16]. These MNs rapidly dissolve upon contact with water when they puncture the skin, thereby resulting in rapid drug delivery. However, some proteins, such as hormones and vaccines, require long exposure times [10, 17, 18]. Therefore, developing a partially dissolving system in which the release rate could be controlled is important for sustained transdermal delivery.

In addition, a variety of dissolving MNs are primarily produced by filling a three-dimensional MN mold using a long centrifugation time to overcome the constraints of surface tension and solution viscosity [19]. The inability to fabricate these dissolving MNs at a large scale will be one of the key barriers to their widespread use. Therefore, an easy, mild, and efficient manufacturing process is necessary. O_2 plasma has been widely used to modify the surfaces of materials, particularly hydrophobic materials [6, 20-22], but the use of this technique has rarely been reported in the processing of MNs. Herein, a novel and simple method was used to fabricate partial dissolving polymer MN patches, in which O_2 plasma was used to modify the PDMS female mold followed by a simple casting process.

A series of PVP/PVA polymer MN patches with different composition ratios could be used to regulate the drug release rate. The characteristics, insertion capability, and in vitro transdermal delivery of model proteins of the PVP/PVA MN patches were investigated in this study. The insertion of polymer MNs was observed in real time using optical coherence tomography (OCT), which is a non-invasive technique for characterizing the skin structure. Herein, OCT was used to visualize, in real time, polymer MN patches while being inserted into skin in vitro, thereby allowing the exact MN penetration depth to be measured. To assess the feasibility of using PVP/PVA MNs to improve the transdermal delivery of macromolecules, rhodamine

6G and fluorescein isothiocyanate-labeled bovine serum albumin (BSA-FITC) were encapsulated within these MNs. The delivery depths of these two model drugs were investigated using confocal microscopy, and the well-established Franz cell system was used to determine the cumulative permeation of the MN patches.

Experimental

Manufacture of partial dissolving polymer MN patches

A commercial MN patch, the 3M™ microchannel skin system (Taho Pharma, Singapore), was used as a master mold for the MN arrays. The dimensions of the MNs on the array were a height of 650 μm with 351 pyramidal needles in a 6 x 13 mm area. The female polydimethylsiloxane (PDMS) (Sylgard 184, Dow Corning, Belgium) molds were manufactured by pouring a PDMS solution over the 3M mold. The PDMS solution was prepared by mixing the elastomer and curing agent in 10:1 w/w ratio, which was followed by vacuuming at -76 cm Hg for 2 hr to remove bubbles and then curing at 80℃ for 30 min. The PDMS mold was then gently peeled off of the 3M master mold.

Polyvinyl alcohol (PVA) (BF-17, CCP) and polyvinylpyrrolidone (PVP) (MW 10 kDa, Sigma-Aldrich, USA) were selected as materials for fabricating the MN arrays. Pure PVA and four different weight ratios of polymer, PVP:PVA (1:1, 1:2, 1:4, 1:6), were prepared in deionized water at a concentration of 15%. Surface modification of the PDMS molds was performed using an O_2 plasma cleaner (Harrick Plasma, USA), and then the polymer solutions were poured into the PDMS molds and dried overnight.

Preparation of PVP/PVA MN patches

As shown in Figure 1(A), the direct casting of a mixed drug and polymer solution was performed in a single step. In this case, the drug was uniformly distributed within the PVP/PVA MN patches after drying. In addition, Figure 1(B) shows the two-step casting process, which consists of first loading and drying the mixed drug and polymer solution followed by pasting to the backing prepared using a 25 % PVP

polymer solution (MW 360 kDa, Sigma-Aldrich, USA) under an ambient air environment. Rhodamine 6G (M.W. 470.01 Da, Sigma-Aldrich), which is a water-soluble red fluorescent dye with excitation/emission peaks at 526/555 nm, was used as a low-molecular-weight model drug and dissolved in DI water to prepare a stock solution with a concentration of 0.5 mg/mL, and then 50 μL of the stock solution was added to the polymer solutions. FITC-BSA (A3059, Sigma-Aldrich, USA), which has excitation/emission peaks at 490/520 nm, was used as a high-molecular-weight model drug. An inverted fluorescent microscope was used to observe the shapes of the drug-loaded MNs and to ensure that the drugs were successfully loaded into the MNs.

Morphology of PVP/ PVA MNs

Stereomicroscopy (Nikon P6000, Japan) and scanning electron microscopy (S-300N, Hitachi, Japan) were used to observe the morphologies and dimensions of the MNs. The detailed dimensions as illustrated in Figure 2(B), including the heights, widths, lengths and interspacings of the polymer MNs, which were analyzed using Image J software and compared with those of the master mold.

In vitro skin penetration studies

To evaluate the in vitro skin insertion capability of the series of MNs with different proportions of PVA/PVP, MN patches with/without loaded rhodamine 6G were inserted into 400 μm of porcine cadaver skin using a homemade applicator with a force of 9.8 N/patch for 30 min and 30 sec and then peeled off, respectively. For the MN patches without loaded rhodamine 6G, after the MN patch was removed, the skin surface was exposed to a blue tissue-marking dye for 1 min to identify the sites of insertion. Then, the blue spots and the red spots on the skin were observed using a

stereomicroscope (Nikon P6000, Japan). The insertion ratio for each test sample was calculated and was defined as the number of red/blue spots on the skin after insertion divided by the number of needles in the arrays, respectively.

Optical Coherence Tomography (OCT)

To evaluate the possibility for inserting the PVA/PVP MNs using an application force of ~9.5 N/patch for 10 min without peeling off, an optical coherence tomography (OCT) system was used in this study with a MEMS-based swept source for visualization of the series of polymer MN arrays. The center wavelength of the swept source (HSL-20, Santec Corp., Japan) is located at 1310 nm with a scanning spectral range of 105 nm, which can provide a deeper imaging depth compared to the 800-nm OCT system. The A-mode scanning rate and the output power can reach values of 100 kHz and 30 mW, respectively. The light source was connected to a Mach–Zehnder interferometer. Ninety percent of the laser output power was connected to the sample arm, and a 10X objective lens (LSM02, Thorlabs) was used in the sample arm to provide a lateral resolution of ~10 μm. In addition, the longitudinal resolution of our OCT system can achieve 7 μm. In our OCT system, the physical area for OCT imaging was approximately 2 × 2 × 3 mm^3, corresponding to 1000 × 500 × 600 voxels. With an A-scan rate of 100 kHz, the frame rate of our OCT system can achieve 100 frames/s, in which each frame consists of 1000 A-scans. The insertion and creation of pores following the application by the series polymer MNs to porcine cadaver skin at a force of 9.8 N/patch for 10 min was investigated using an OCT scanner (OCT, Chang Gung University, Taiwan). The penetration depths were evaluated immediately without histological sections.

Imaging of in vitro transdermal delivery of rhodamine 6G and FITC-BSA to rat ear skin

Rhodamine 6G-loaded MN patches and FITC-BSA loaded-MN patches were applied to rat ear skin, and these patches were removed from the skin after administration for 10 min and 30 min, respectively. The penetration of rhodamine 6G and FITC-BSA in the skin to the vertical direction of the rat ear skin, full-thickness skin was placed on a slide and investigated by using confocal microscope (LSM 510 META, Zeiss, Germany). Images were obtained in the xy-plane (parallel to the plane of the rat ear skin surface). The initially scanned position of the skin surface (z=0 μm) was defined as the imaging plane with the brightest fluorescence. Scanning was conducted once at the interval of 10 μm for PVP/PVA=1:4 MN patches and 20 μm for PVP/PVA=1:1 MN patches from skin surface through the z-axis perpendicular to the xy-plane. The 3D confocal reconstruction images were also obtained to visualize the penetration of drug release into the skin.

In vitro transdermal delivery of rhodamine 6G and FITC-BSA

In vitro transdermal delivery studies were performed using Franz diffusion cells (chin-Fa, Taiwan). Rhodamine 6G-loaded MN patches and FITC-BSA-loaded MN patches were inserted into porcine cadaver skin. The stratum cornea side of the skin was exposed to ambient conditions, whereas the dermal side was kept facing the receptor solution. The receptor medium (5.5 ml of 1X PBS, pH 7.4) was maintained at 32℃ in an incubator and continuously stirred at a speed of 600 rpm. The drug-loaded MN patch was fixed to occlusive adhesive tape (1516 Poly Med, 3M) and applied into the skin with a constant application force of 9.8 N. The receptor medium was analyzed at each time point using a spectrofluorometer. The cumulative permeation amounts of rhodamine 6G and FITC-BSA extracted from the MN patches were determined from the solution. The reading value was fitted to the standard curves of rhodamine 6G and FITC-BSA to obtain the actual concentration of the drug delivery

solution.

Results and Discussion

Characterization of PVP/PVA MNs

The original 3M molds have been used to provide a simple way to create channels in the stratum corneum without the need for expensive powered devices [23]. In addition, Lee et al. reported that using pyramidal MNs with a small aspect ratio can provide better mechanical strength than conical-type MNs for mechanically weak biomaterials such as Carboxymethyl cellulose [24]. Therefore, 3M molds with a pyramidal shape were selected as the master mold to fabricate a series of PVP/PVA MN patches with encapsulated model drugs in different proportions for in vitro penetration. In addition, a mild and easy method, in which O_2 plasma treatment was used to modify the PDMS surface followed by a simple casting process, was employed to fabricate partial dissolving polymer MN patches. Because the hydrophobic nature of the PDMS surface prevents polymer solution casting, surface modification is essential. In previous literatures, different kinds of surface modifications have been used to improve the wettability of PDMS for biomedical application, including oxygen plasma[25-27]. It is revealed that the surface properties of PDMS can be easily converted from a hydrophobic to a hydrophilic state by exposure to oxygen or low pressure air plasma [25]. After treatment with plasma, surface methyl groups are removed and replaced with hydroxyl groups and convert the surface wettability [28].

Previous studies have fabricated polymeric MNs which could be dissolved or degrade in the skin after insertion have melted polymer into the mold at high temperature or dissolved in organic solvent, which may damage the activity of

biomolecules[29] . As illustrated in Figure 1, process A consisted of directly casting a mixed drug and polymer solution, and process B minimized the drug waste and localized the drug in the needle. This mild processing method provided the following advantages: preservation of the activity of the incorporated molecule during processing, the high encapsulation of drugs, and the ability for scaling up.

The theoretical dimensions of the 3M molds were as follows: height of 650 μm, width of 300 μm at the base, and interspacing of 250 μm. As shown in Figures 2(A) and 2(B), a series of PVA and PVP/PVA MNs were successfully replicated from the 3M MNs. A diagrammatic representation of a MN array and its geometrical parameters are presented in Figure 2(C), and the detailed dimensions of each PVP/PVA needle are shown in Figure 2(D). As shown in Figure 2(D), there are 10% height losses of sequential MNs were investigated. It is suggested that the properties of polymer solution may affect the dimension of polymeric MNs, such as the hydrophilic property, polymer-PDMS interaction, and the viscosity. Furthermore, since there are several factors affect the insertion ability of MN patches, the shape and aspect ratio are primarily discussed. In this study, the aspect ratios of the series of MN patches were almost close to that of the original 3M mold. However, the aspect ratio of the MNs prepared by 15% PVA is 2.45 which was little lower than others. Lee et al., have revealed that the relatively wide base (i.e., 300μm) and small aspect ratio (i.e.,2) of the pyramidal MNs may contribute to the insertion [24]. Previous study also demonstrated that aspect ratio may be a crucial parameter in influencing the mechanical properties of MNs[11]. Although there are a little different between sequential MNs and original 3M mold, it is considered that the 600μm in height is enough for insertion.

Insertion capability of PVP/PVA MN patches

To compare the skin insertion capabilities of the series of MN patches with different proportions of PVP/PVA MNs with/without loaded rhodamine 6G were inserted into porcine cadaver skin, and these MNs were removed after 30 sec and 30 min of insertion, respectively. Stereomicroscopy images of the porcine cadaver skin after insertion are shown in Figure 3(a1-d1 and a2-d2). The insertion ratio for each sample was calculated by dividing the number of blue spots and red spots on the skin after insertion by the number of needles in the arrays, respectively. As shown in Figure 3(a1-d1), these spots cannot be washed away, which indicated that the red dye of rhodamine 6G was located within the porcine skin. The resulting red spots revealed a high insertion ratio in each PVP/PVA MNs (greater than 98%). In addition, the red spot pattern also demonstrated that the red color spread out as the content of PVP increased, which is shown more clearly in the magnified image. To visualize the holes in the porcine skin caused by the MN patches, polymer MN patches without loaded rhodamine 6G were also inserted into porcine skin for 30 seconds, and the test skin was stained with a blue tissue-marking dye that selectively marked the sites of the pierced skin to calculate the insertion ratio. As shown in Figure 3(a2-d2), the insertion result was consistent with that shown in Figure 3(a1-d1). Furthermore, Figure 3(a3-d3) presents images of the series of PVP/PVA MN patches after insertion. It is also clearly observed that the mechanical strength of the MN array decreased as the PVP content increased which is also consistent with S1. Since the PVP could be dissolved in the water when the MN inserted, the dissolving part increased as the PVP content increased which resulted in the mechanical strength decreased. Although the mechanical strength decreased as the PVP content increased, it is revealed that the insertion ratio of PVP/PVA=1:1 was closed to the 100% which demonstrated that the needles also have sufficient strength.

Optical coherence tomography

In addition, to obtain real-time images of the insertion, a noninvasive optical imaging technique, OCT, was used in this study to investigate the insertion of these polymeric MN patches in the porcine skin, and the images are shown in Figure 4. The 2D top-view images and side-view images of a series of PVP/PVA MNs inserted into porcine skin are shown in Figure 4(A). In addition, the MNs punctured the stratum cornea barrier, and the holes formed by the PVP/ PVA MN patches are also shown in the 3D reconstruction images in Figure 4(B). These results indicated that the series of PVP/ PVA MN patches all possessed the capability to insert into the porcine skin and that the ability to puncture the skin was enhanced as the PVP content decreased. Moreover, the OCT analysis demonstrated that these partial dissolving polymer MN arrays penetrated to a depth of approximately 250~300 μm, as determined from the cross section view, and created pores with a surface diameter of approximately 200~250 μm, as determined from the top view. The en-face images at a depth of 300 μm beneath the tissue surface also confirmed the penetration ability of these MN arrays. Because the proportion of PVP/PVA affects the drug release rate, to consider the balance of release efficiency and insertion capability, the 1:4 and 1:1 groups were chosen for subsequent studies. Note that the non-invasive imaging technique facilitated the real-time functional imaging of skin in the natural state and that the tissue was not sacrificed for in vivo study in future applications.

In vitro release profiles of rhodamine 6G-loaded and BSA-FITC-loaded PVP/PVA microneedle patches

To study the release profiles of the encapsulated model drug from PVP/PVA MNs, rhodamine 6G-loaded MN patches (Figures 6a and 6b) and the patch without needles

were inserted into porcine cadaver skin and the drug release was monitored for 3 days. Polymer MN patches of PVP/PVA=1:4 and PVP/PVA=1:1 were inserted into porcine skin. The permeation profiles of rhodamine 6G released from the polymer MN arrays and from the patch that contained only the same drug loading across the skin were determined, as shown in Figure 6c. In comparison to the patch without the MN array group, the PVP/PVA=1:4 and PVP/PVA=1:1 MN arrays delivered more drug across the skin over a period of approximately 6 hours, and the cumulative permeation amounts reached 200 μg and 450 μg after 3 days, respectively. In contrast, the quantification of delivered drug from the patch without the MN array is only approximately 10% of the patches with the MN array over the same period. In addition, as shown in Figure 6c, both the 1:1 and 1:4 MN array curves exhibited linear and sustain release, and the amounts of drug released were regulated by the composition.

Moreover, to study the release profiles of the PVP/PVA MN patch loaded with a large protein, BSA-FITC-loaded MN patches (Figures 8a and 8b) were inserted into porcine cadaver skin and the drug release was monitored for 5 days. The amounts of drug released from the PVP/PVA=1:4 and PVP/PVA=1:1 MN patches were compared, and the permeation profiles of BSA-FITC released from the polymer MN arrays are shown in Figure 8c. As shown, BSA-FITC is a large protein with a molecular weight of 66 kDa, and its release efficiency is lower than that of rhodamine 6G. In addition, both the 1:1 and 1:4 MN array curves exhibited linear and sustained release, and the amounts of drug released were regulated by the composition, which is consistent with Figure 6c. Therefore, the results demonstrate that the PVP/PVA MNs significantly assist the delivery of the drug and that the composition of the polymer blend may achieve controlled release.

In vitro transdermal delivery of rhodamine 6G and FITC-BSA to rat ear skins

To evaluate the feasibility for transdermal delivery of rhodamine 6G and BSA-FITC, PVP/PVA MNs loaded with these drugs were inserted into rat ear skin and observed using confocal microscopy. Both PVP/PVA=1:4 and PVP/PVA=1:1 MN patches were compared, and the penetrations of released rhodamine 6G and BSA-FITC across the skin at varying depths after insertion for 10 min and 30 min were investigated, respectively. To visualize the penetration of rhodamine 6G and BSA-FITC in the vertical direction of the rat ear skin, the skin puncture sites were imaged and scanned at varying depths from the skin surface using confocal microscopy. For the delivery of rhodamine 6G, as shown in Figure 5, the maximum penetration depths observed in the skin at 10 min for PVP/PVA=1:4 and PVP/PVA=1:1 MN were approximately 190 μm (Figure 5A) and 380 μm (Figure 5B), respectively. Because the insertion time was only 10 min, it is suggested that the MN punctured the stratum cornea and extended more than 250 μm. Furthermore, for the delivery of BSA-FITC, as shown in Figure 7, the maximum penetration depths observed in the skin at 30 min for PVP/PVA=1:4 and PVP/PVA=1:1 MN were approximately 90 μm (Figure 7A) and 120 μm (Figure 7B), respectively. The vertical images also demonstrated that the release rate is controlled by the PVP content. The mechanism of the drug release style could be suggested as follow: after insertion, the PVP dissolving in the skin resulted in the drug release. Then, the PVA swelling enhanced the sustained release of the drugs. Because BSA-FITC is a high-molecular-weight protein, it is hypothesized that its release rate is slower than that of rhodamine 6G. Besides the molecular weight effect, different fabricated process may also affect the diffusion. It is considered that molecular weight is the most important factor on the diffusion, but the patch with drugs may result in the

concentration gradient effect and assist the diffusion of rhodamine 6G. Lee et al., have used the backing membrane as a drug reservoir and revealed drug diffusion may enhance by hydrating the backing layer with interstitial fluid from the skin through channels created by MNs [24].However, the drug delivery mechanism of two systems need to discuss further. The results also indicate that the MNs assist the hydrophilic drug and protein across the stratum cornea and enhance the drug delivery. The pair of partial dissolving materials used to fabricate the polymer MN patches may provide good regulation for controlled drug release.

Conclusions

This study demonstrated a plasma treatment that is capable of fabricating partial dissolving MN patches through the use of mild and simple methods without the need for a long centrifugation process. This two-stage mild fabrication process enabled the encapsulation of fragile macromolecules and localized the drug in the needle to minimize drug loss. This method could control the drug release rate by varying the PVP/PVA composition. In addition, OCT imaging enabled real-time functional imaging of skin penetration in the natural state and provided the penetration depth data without the need for tissue sections. In conclusion, the plasma treatment process provides a new solution to the problems encountered in the conventional techniques for fabricating partial dissolving MN patches, thereby providing potential for use as a drug-delivery system for macromolecules such as proteins, hydrophilic drugs, and vaccines.

Acknowledgements

We acknowledge financial support from Chang Gung University and Summit Project Grants of the Chang Gung Memorial Hospital (Grants: CMRPD1C0432 -to I-Chi Lee). We also acknowledge instrument support from Mu-Yi Hua (Department of

Chemical and Materials Engineering, Chang Gung University) and technique support from Mei-Chin Chen and Shau-Wei Tsai.

Supporting Information Section

Fig S1. shows the Mechanical behavior of dissolving PVP/PVA MNs. Supplementary data associated with this article is available free of charge via the Internet.

References

1. S. Khafagy el, M. Morishita, Y. Onuki and K. Takayama, *Advanced drug delivery reviews*, 2007, 59, 1521-1546.
2. S. Coulman, C. Allender and J. Birchall, *Critical reviews in therapeutic drug carrier systems*, 2006, 23, 205-258.
3. M. J. Garland, K. Migalska, T. M. Mahmood, T. R. Singh, A. D. Woolfson and R. F. Donnelly, *Expert review of medical devices*, 2011, 8, 459-482.
4. B. Al-Qallaf and D. B. Das, *Annals of the New York Academy of Sciences*, 2009, 1161, 83-94.
5. M. M. Badran, J. Kuntsche and A. Fahr, *European journal of pharmaceutical sciences : official journal of the European Federation for Pharmaceutical Sciences*, 2009, 36, 511-523.
6. K. Tsioris, W. K. Raja, E. M. Pritchard, B. Panilaitis, D. L. Kaplan and F. G. Omenetto, *Advanced functional materials*, 2012, 22, 330-335.
7. L. Y. Chu, S. O. Choi and M. R. Prausnitz, *Journal of pharmaceutical sciences*, 2010, 99, 4228-4238.
8. M. J. Garland, E. Caffarel-Salvador, K. Migalska, A. D. Woolfson and R. F. Donnelly, *Journal of controlled release : official journal of the Controlled Release Society*, 2012, 159, 52-59.
9. X. Hong, L. Wei, F. Wu, Z. Wu, L. Chen, Z. Liu and W. Yuan, *Drug design, development and therapy*, 2013, 7, 945-952.
10. J. W. Lee, S. O. Choi, E. I. Felner and M. R. Prausnitz, *Small*, 2011, 7, 531-539.
11. M. C. Chen, M. H. Ling, K. Y. Lai and E. Pramudityo, *Biomacromolecules*, 2012, 13, 4022-4031.
12. M. H. Ling and M. C. Chen, *Acta biomaterialia*, 2013, 9, 8952-8961.
13. S. P. Sullivan, D. G. Koutsonanos, M. Del Pilar Martin, J. W. Lee, V. Zarnitsyn, S. O. Choi, N. Murthy, R. W. Compans, I. Skountzou and M. R. Prausnitz, *Nature medicine*, 2010, 16, 915-920.
14. C. J. Ke, Y. J. Lin, Y. C. Hu, W. L. Chiang, K. J. Chen, W. C. Yang, H. L. Liu, C. C. Fu and H. W. Sung, *Biomaterials*, 2012, 33, 5156-5165.
15. L. Guo, J. Chen, Y. Qiu, S. Zhang, B. Xu and Y. Gao, *International journal of pharmaceutics*, 2013, 447, 22-30.
16. A. Nayak, D. B. Das and G. T. Vladisavljevic, *Pharmaceutical research*, 2014, 31, 1170-1184.
17. J. M. Kemp, M. Kajihara, S. Nagahara, A. Sano, M. Brandon and S. Lofthouse, *Vaccine*, 2002, 20, 1089-1098.
18. H. H. Kwak, W. S. Shim, M. K. Choi, M. K. Son, Y. J. Kim, H. C. Yang, T. H. Kim, G. I. Lee, B. M. Kim, S. H. Kang and C. K. Shim, *Journal of controlled release : official journal of the Controlled Release Society*, 2009, 137, 160-165.
19. M. G. McGrath, S. Vucen, A. Vrdoljak, A. Kelly, C. O'Mahony, A. M. Crean and A. Moore, *European journal of pharmaceutics and biopharmaceutics : official journal of Arbeitsgemeinschaft fur Pharmazeutische Verfahrenstechnik e.V*, 2014, 86, 200-211.
20. R. K. Pirlo, X. Peng, X. Yuan and B. Z. Gao, *Optoelectronics letters*, 2008, 4, 387-390.
21. V. Rodriguez-Santiago, L. Vargas-Gonzalez, A. A. Bujanda, J. A. Baeza, M. S.

Fleischman, J. H. Yim and D. D. Pappas, *ACS applied materials & interfaces*, 2013, 5, 4725-4730.
22. Y. Sun, M. Krishtab, H. Struyf, P. Verdonck, S. De Feyter, M. R. Baklanov and S. Armini, *Langmuir : the ACS journal of surfaces and colloids*, 2014, 30, 3832-3844.
23. D. Duan, C. Moeckly, J. Gysbers, C. Novak, G. Prochnow, K. Siebenaler, L. Albers and K. Hansen, *Current drug delivery*, 2011, 8, 557-565.
24. J. W. Lee, J. H. Park and M. R. Prausnitz, *Biomaterials*, 2008, 29, 2113-2124.
25. D. A. Markov, E. M. Lillie, S. P. Garbett and L. J. McCawley, *Biomedical microdevices*, 2014, 16, 91-96.
26. S. Pinto, P. Alves, C. M. Matos, A. C. Santos, L. R. Rodrigues, J. A. Teixeira and M. H. Gil, *Colloids and surfaces. B, Biointerfaces*, 2010, 81, 20-26.
27. S. H. Tan, N. T. Nguyen, Y. C. Chua and T. G. Kang, *Biomicrofluidics*, 2010, 4, 32204.
28. K. Efimenko, W. E. Wallace and J. Genzer, *Journal of colloid and interface science*, 2002, 254, 306-315.
29. J. H. Park, M. G. Allen and M. R. Prausnitz, *Pharmaceutical research*, 2006, 23, 1008-1019.

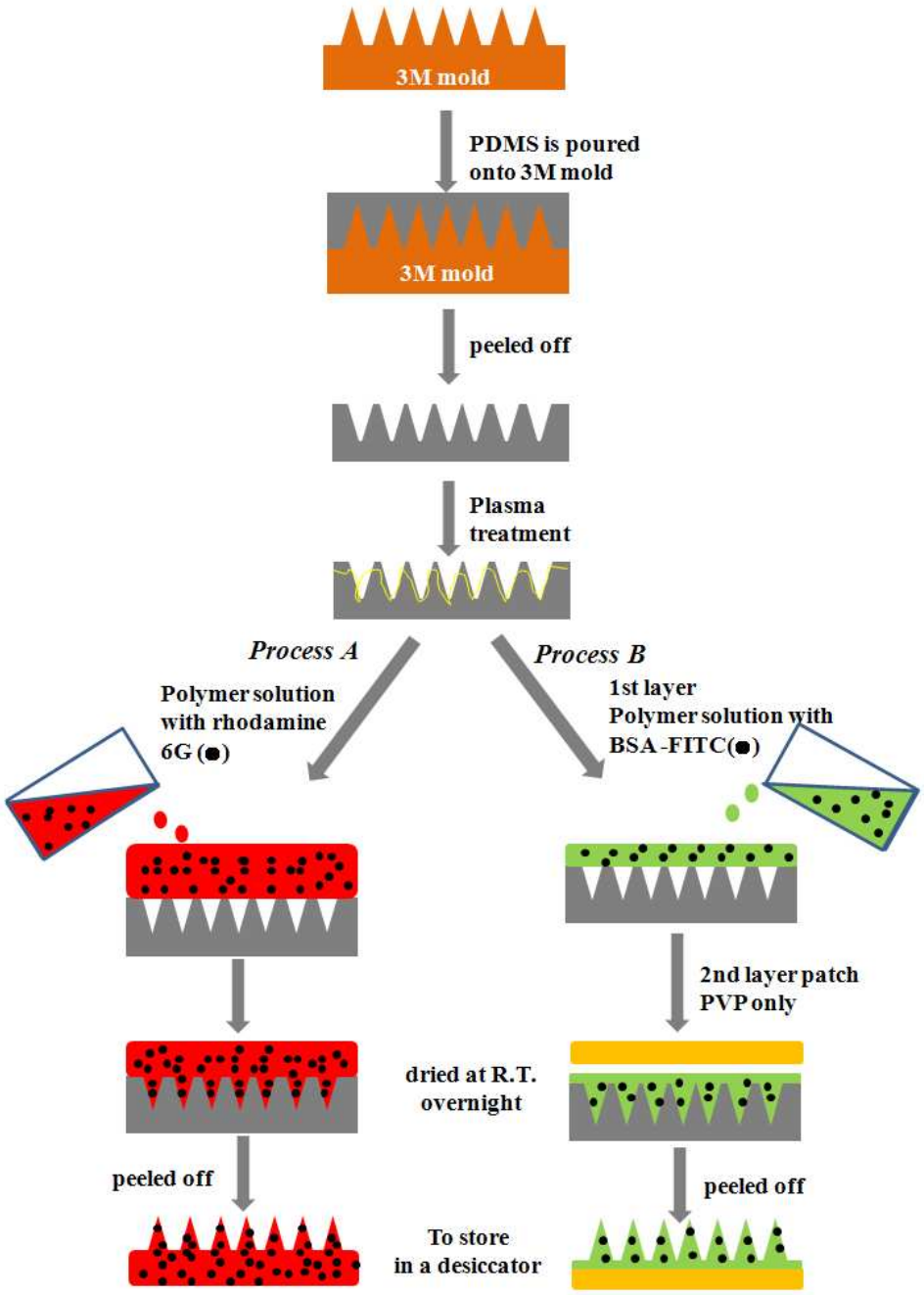

Figure 1. Schematic illustration of the process for fabricating PVP/PVA MN patches. Process A illustrates the one-stage fabrication of PVP/PVA MNs, and the entire MN patch encapsulated the model drug rhodamine 6G. Process B illustrates the two-stage fabrication of PVP/PVA MNs, and only the base patch encapsulated the model drug BSA-FITC.

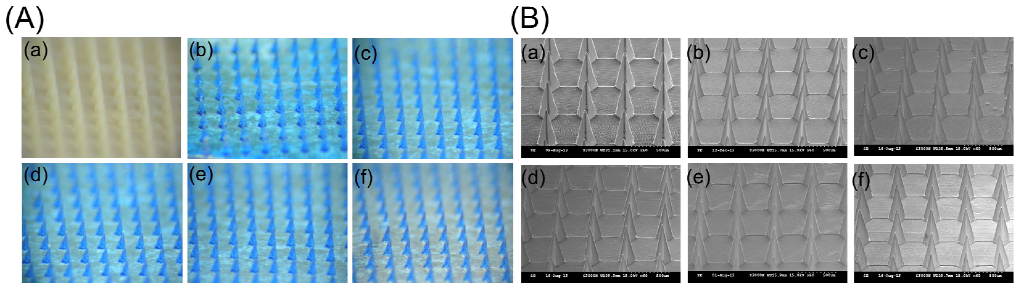

(C)

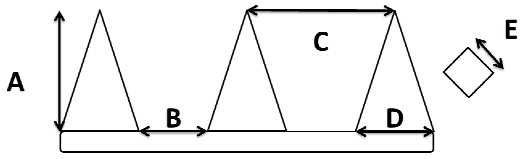

Aspect ratio = A / D（Height / Width）

A : Height of MNs in array
B : Interspacing of MN at base
C : Interspacing of MN at tip
D : Width of MN at base
E : Length

(D)

Material	(A) Height (μm)	(B) Interspacing Base (μm)	(C) Interspacing tip (μm)	(D) Width (μm)	(E) Length (μm)	Aspect ratio
3M Mold	650.00	233.90±5.24	515.95±11.04	272.79±6.85	184.10±2.60	2.38
PVA= 15%	594.30±26.25	239.73±9.93	472.79±13.64	242.51±3.98	160.52±8.75	2.45
PVP:PVA =1:1	595.28±15.19	241.47±19.95	472.44±22.84	213.84±6.77	170.64±6.78	2.76
PVP:PVA =1:2	592.69±17.15	240.33±9.81	473.31±9.94	226.66±10.82	160.88±7.45	2.67
PVP:PVA =1:4	630.35±16.67	232.59±9.06	468.47±10.91	229.30±12.36	159.96±9.96	2.75
PVP:PVA =1:6	600.25±18.03	243.57±10.49	460.91±9.68	222.20±5.61	155.10±3.61	2.68

Figure 2. Detailed dimensions of sequential PVP/PVA MNs. (A) Stereomicroscopy images; (B) Scanning electron microscopy images of PVP/PVA MN patches: a) 3M mold, b) 15% PVA, c) PVP/PVA = 1:6, d) PVP/PVA = 1:4, e) PVP/PVA = 1:2, and f) PVP/PVA = 1:1; (C) Diagrammatic representation of a MN array and its geometrical parameters; (D) Physical characteristics of MN arrays prepared from a series of PVP/PVA using a 3M mold.

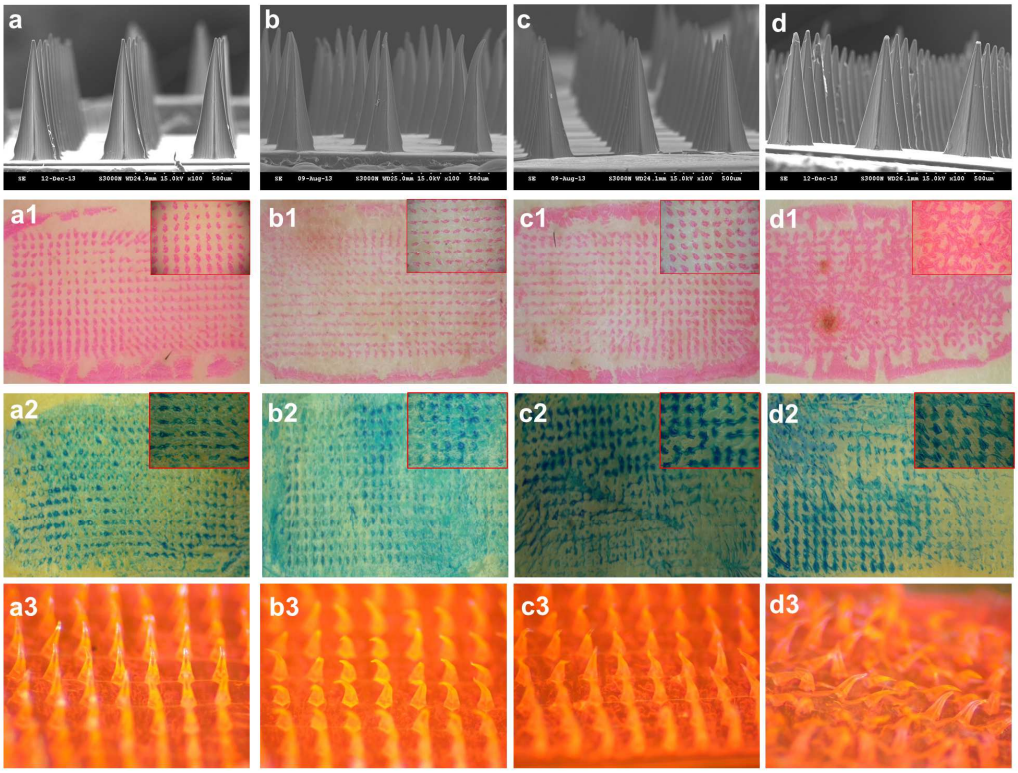

Figure 3. In vitro skin insertion capability of rhodamine 6G-loaded PVP/PVA MN patches. a-a2) 15% PVA, b-b2) PVP/PVA = 1:6, c-c2) PVP/PVA = 1:4, d-d2) PVP/PVA = 1:1. Scanning electron microscopy images of PVP/PVA MN patches (a-d), porcine cadaver skin after the insertion of PVP/PVA MN patches loaded with rhodamine 6G after 30 min (a1-d1) and porcine cadaver skin after insertion and staining with tissue marking dye (a2-d2). Magnified images are also shown in a1-d1 and a2-d2. Stereomicroscopy images of PVP/PVA MN patches after insertion (a3-d3).

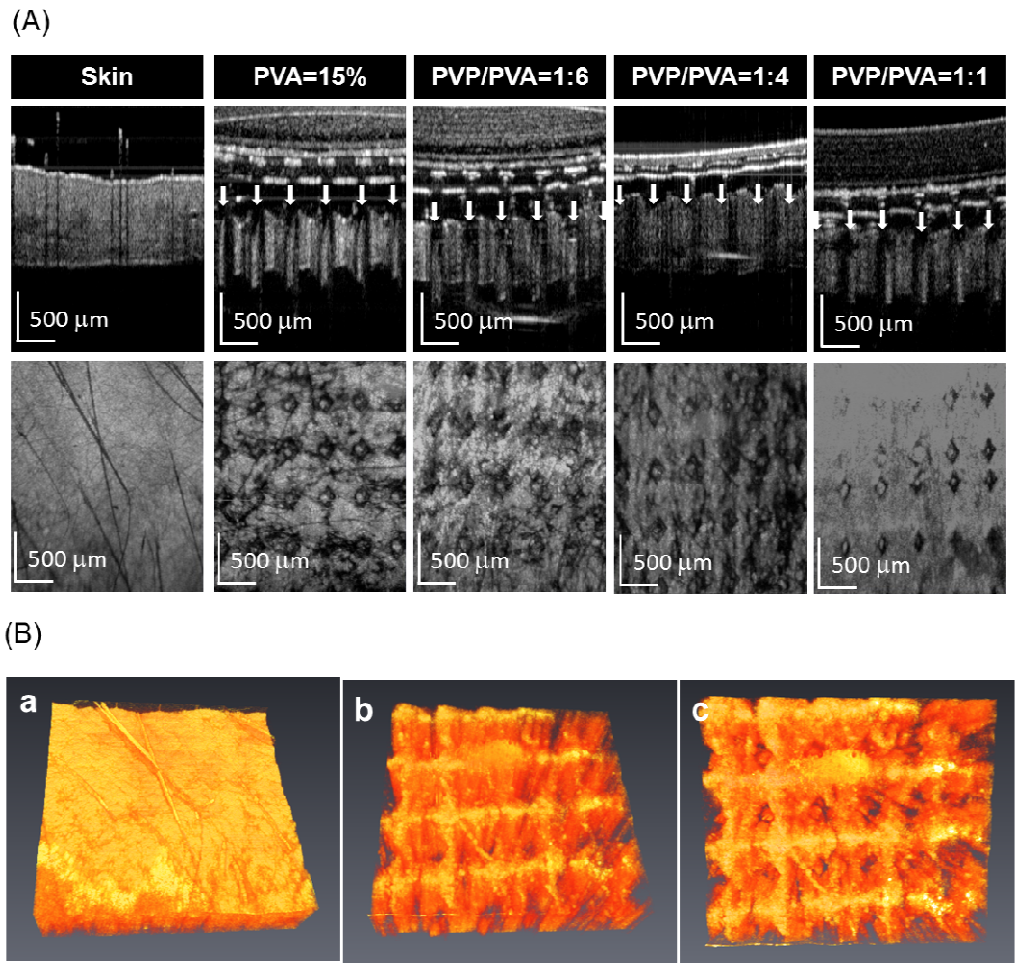

Figure 4. Representative OCT images highlighting the ability of PVP/PVA MN patches to penetrate into porcine skin. (A). 1st row is 2D images of the cross section, and 2nd row is en-face images at a depth of 300 μm beneath the tissue surface. White arrows highlight the location of microdisruptions in the skin. (B) 3D reconstruction images of (a) porcine skin, (b) PVP/PVA = 1:4 of degree of 45, and (c) PVP/PVA = 1:4 of top view.

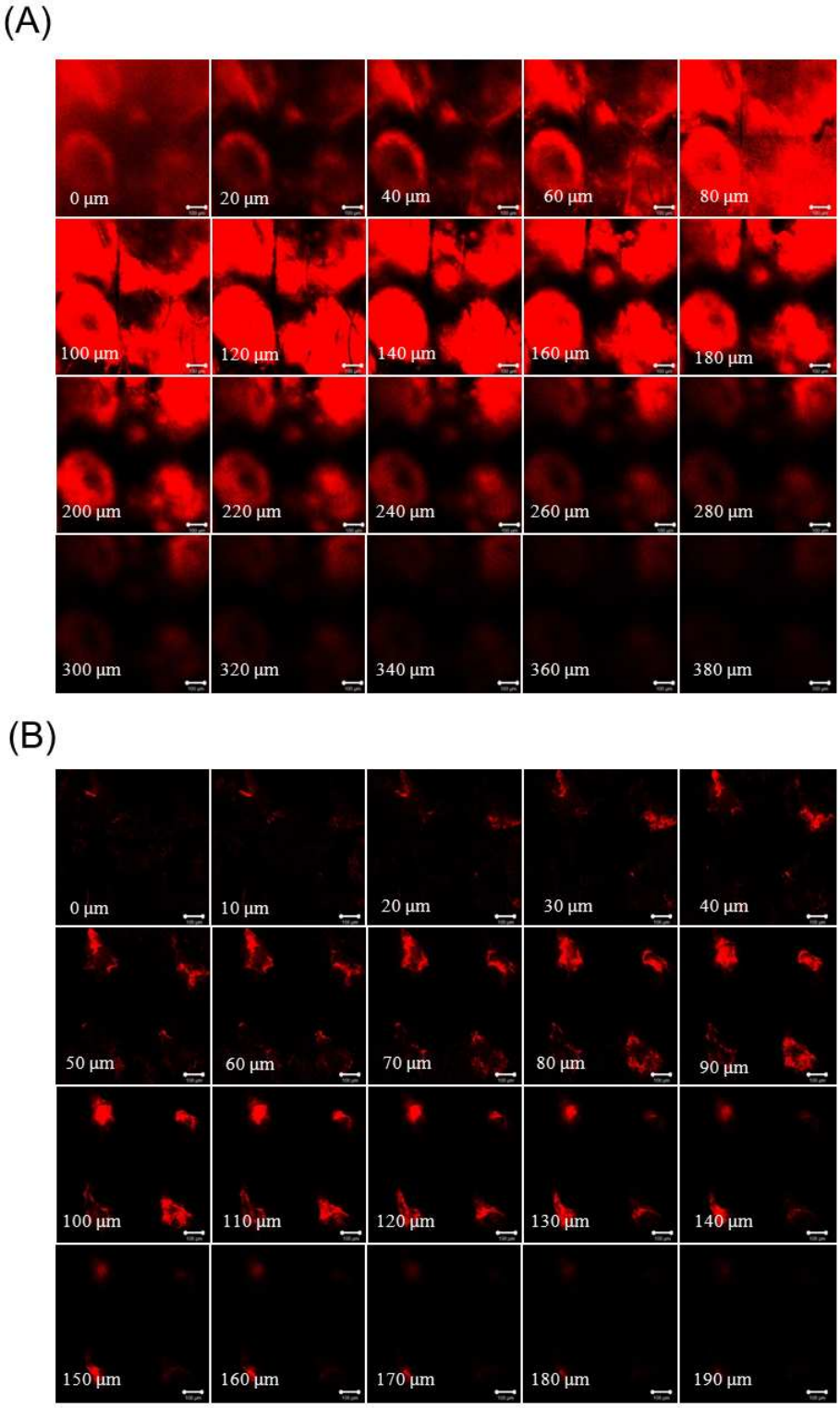

Figure 5. In vitro transdermal delivery of rhodamine 6G-loaded PVP/PVA MNs across the rat ear skin at varying depths after insertion for 10 min. (A)

PVP/PVA = 1:1 MN patches and (B) PVP/PVA = 1: 4 MN patches. The amount of rhodamine 6G loaded in the PVP/PVA MNs was 4500 μg per patch.

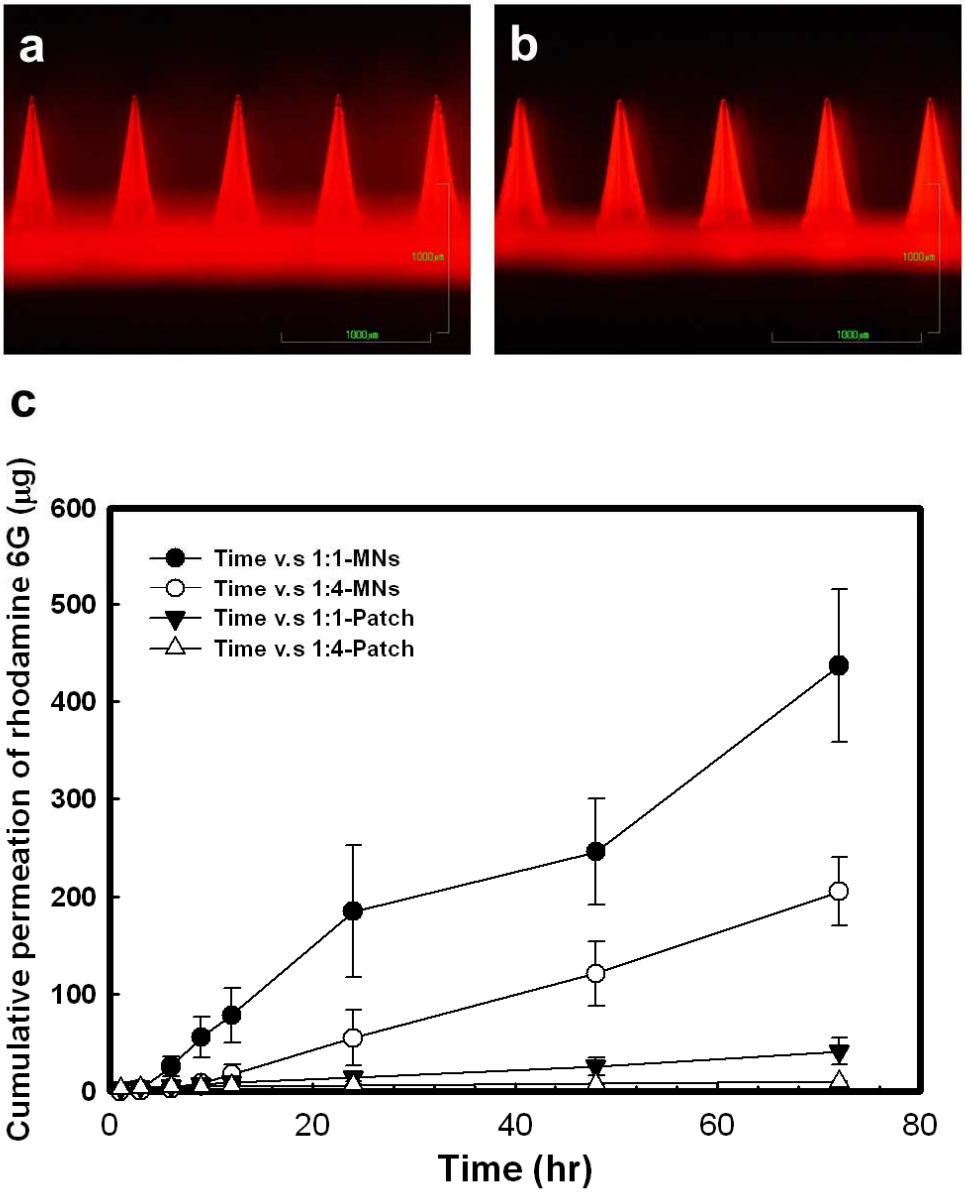

Figure 6. In vitro transdermal delivery of rhodamine 6G-loaded PVP/PVA MNs to porcine ear skin of PVP/PVA = 1:4 MN patches a), and PVP/PVA = 1: 1 MN patches b). Fluorescence images of a-b and stereomicroscopy images of a-b are shown. c. In vitro drug-release profiles.

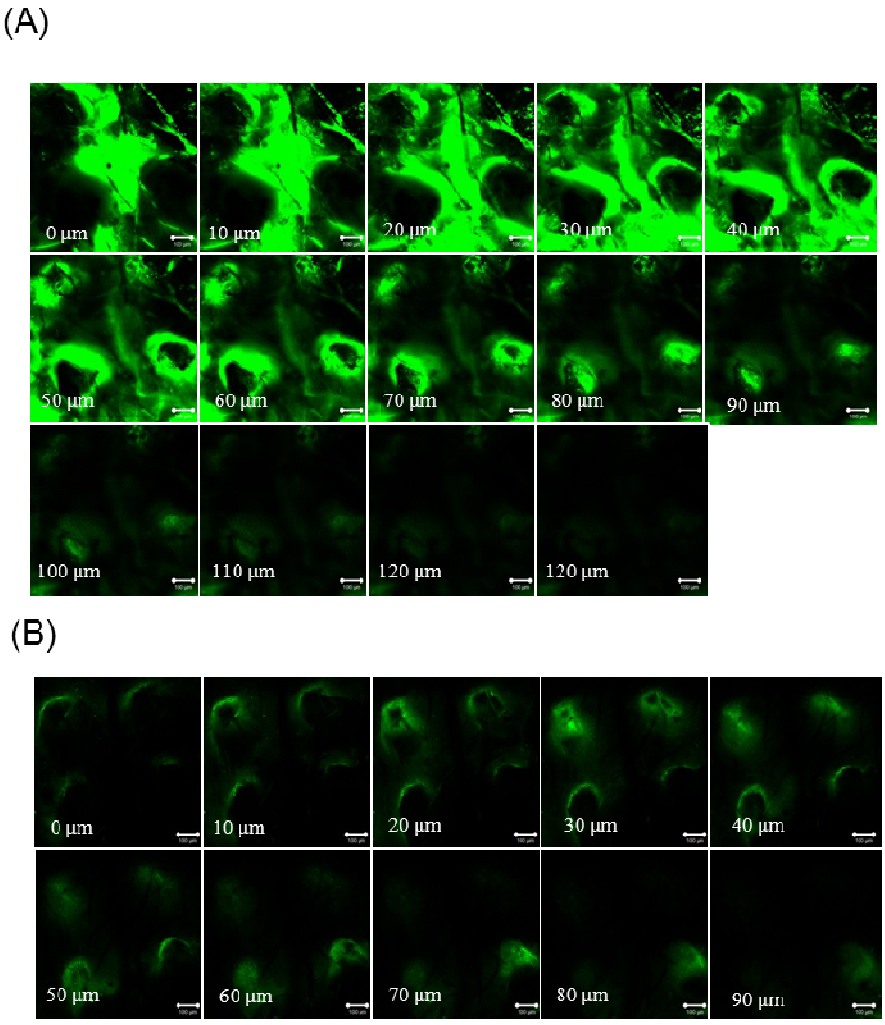

Figure 7. In vitro transdermal delivery of BSA-FITC-loaded PVP/PVA MNs across the rat ear skin at varying depths after insertion for 30 min. (A) BSA-FITC-loaded PVP/PVA=1:1 MN patches and (B) BSA-FITC-loaded PVP/PVA=1:4 MN patches.

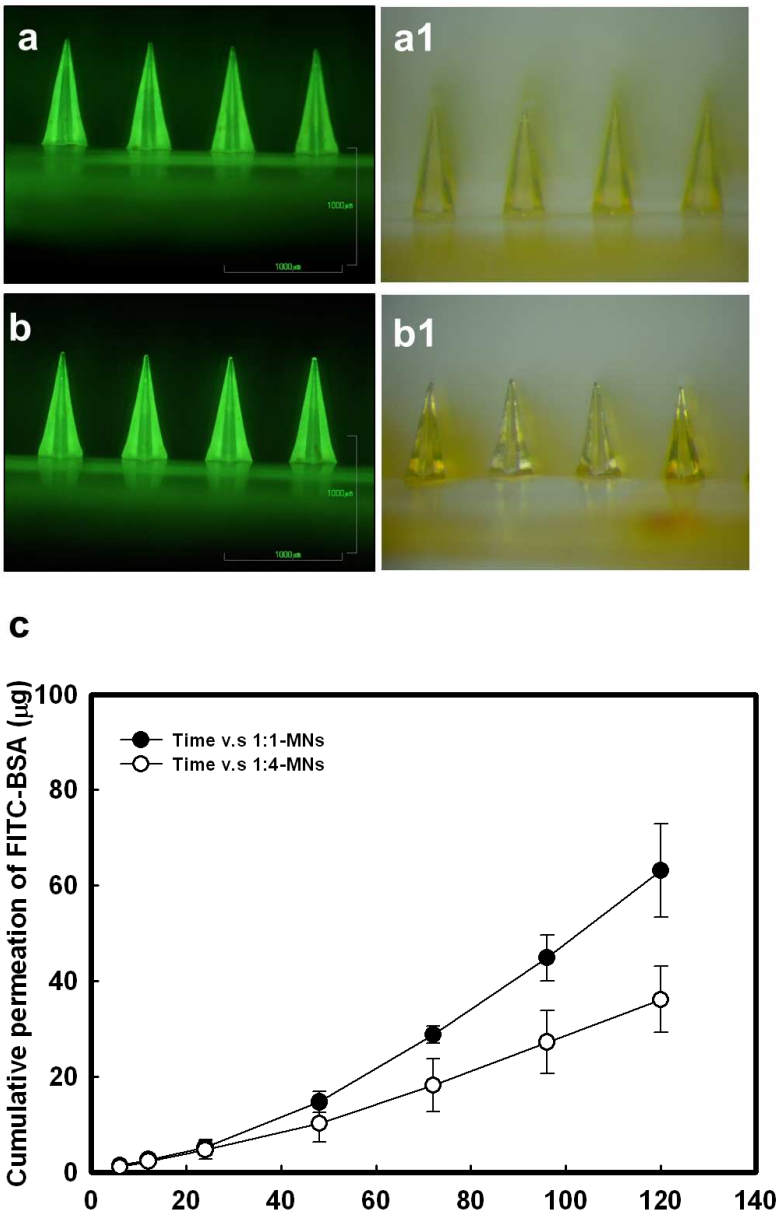

Figure 8. In vitro transdermal delivery of BSA-FITC-loaded PVP/PVA MNs to porcine ear skin by PVP/PVA = 1:4 MN patches a-a1) and PVP/PVA = 1: 1 MN patches b-b1). Fluorescence images of a-b and stereomicroscopy images of a1-b1 are shown. c. In vitro drug-release profiles.

Table of Contents entry:

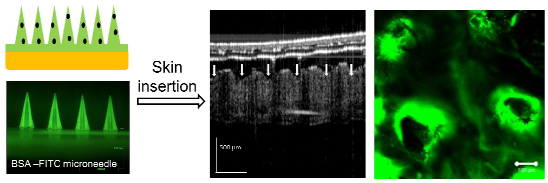

Polymeric MN patches was fabricated by an easy process with O_2 plasma treatment, and efficient, sustained transdermal delivery was achieved.